Double difference tomography for breast ultrasound sound speed imaging

Cuiping Li, Neb Duric, Olsi Rama, Angelika Burger, Lisa Polin and Nicole Nechiporchik

Karmanos Cancer Institute, 4100 John R. Street, 4 HWCRC, Detroit, MI 48201; Phone: 313-576-8768, Emails: lic@karmanos.org

ABSTRACT

Breast ultrasound tomography is a rapidly developing imaging modality that has the potential to impact breast cancer screening and diagnosis. Double difference (DD) tomography utilizes more accurate differential time-of-flight (ToF) data to reconstruct the sound speed structure of the breast. It can produce more precise and better resolution sound speed images than standard tomography that uses absolute ToF data. We apply DD tomography to phantom data and excised mouse mammary glands data. DD tomograms demonstrate sharper sound speed contrast than the standard tomograms.

Keywords: Double difference, tomography, ultrasound breast imaging.

1. INTRODUCTION

Recent studies have demonstrated the effectiveness of ultrasound tomography imaging in detecting breast cancer. The quality of standard tomography largely relies on the accuracy of the picked absolute time-of-flights (ToFs). Recent geophysical applications have shown substantial improvements in the accuracy of reconstruction and earthquake location using differential ToF data.

The DD method was originally developed to optimally relocate seismic events in the presence of measurement errors and earth model uncertainty[1, 2]. The fundamental equation of this iterative least-squares procedure relates the residual between the observed and predicted ToF difference for pairs of earthquakes observed at common stations to changes in the vector connecting their hypocenters with the unknown[3, 4]. The algorithm naturally accepts differential ToFs as data. Based on DD earthquake location method, Zhang and Thurber[3-7] have developed a new seismic tomography method that makes use of waveform cross correlated DD data. They applied DD tomography to both synthetic models and real earth velocity models and the obtained results are superior to that from standard tomography[3-7].

DD tomography relies on the accurate calculation of the relative ToF shift for similar waveforms. In this paper, we explore the application of DD tomography to medical ultrasound sound speed imaging with a toroidal ultrasound array. Our toroidal array acquisition geometry is ideal for the application of the DD method. The use of the waveform cross correlated DD data removes most of systematic error in the data for inversion, which in turn removes some “fuzziness” from the sound speed images. To demonstrate the effectiveness of the method, we have applied it to data acquired by our toroidal array for a breast phantom, a gelatin phantom and 6 excised mouse mammary glands.

In this paper, we review DD tomography method. We also demonstrate some inversion results and comparisons between sound speed images with DD tomography and standard tomography. Finally, we also discuss the potential advantages of DD tomography.

Medical Imaging 2011: Ultrasonic Imaging, Tomography, and Therapy, edited by Jan D'hooge, Marvin M. Doyley,
Proc. of SPIE Vol. 7968, 796802 · © 2011 SPIE · CCC code: 1605-7422/11/$18 · doi: 10.1117/12.877559

2. METHODOLOGY

2.1 Data acquisition

Data was acquired using a clinical prototype located at Karmanos Cancer Institute (KCI) in Detroit, MI. The current prototype employs a toroidal array with 256 evenly distributed ultrasound sensors. Array elements sequentially emit fan beams of ultrasound signals towards the opposite side of the ring. The scattered (transmission) and backscattered (reflection) ultrasound signals are subsequently recorded by all 256 elements at a sampling rate of 8.33 MHz. The transmitted broadband ultrasound signal has a central frequency around 2 MHz. The toroidal array resides in a tank filled with water for proper coupling of the ultrasound signal (Fig. 1).

In this study, we conduct ultrasound scans on breast phantom, gelatin phantom and excised mouse mammary glands with the toroidal array as described above. Although true structures and properties of in vivo breasts are uncertain, those of breast phantom can be obtained during its manufacturing or aggressive imaging methods (e.g. X-ray CT). Therefore, we can use breast phantom scans to benchmark our tomography method. These data are reconstructed using both DD tomography and standard tomography. We will show some examples and compare images resulting from both methods.

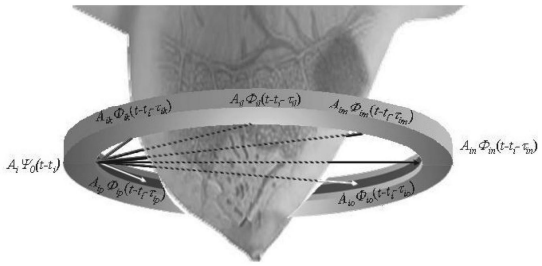

Figure 1. A schematic representation of the toroidial ring transducer.

2.2 DD tomography

DD ultrasound tomography is based on the assumption that physically adjacent waveforms are similar and cross correlations can then be used to determine precise differential ToFs between them. Our toroidal array acquisition geometry is ideal for the application of the DD method. In this study, differential ToF data for DD tomography can be calculated in a circular geometry, which, in the sense of homogeneity of data coverage, is superior to linear array. We cross correlate 18 nearby waveforms of both common transmitter gather and common receiver gather, to get differential ToF data for sound speed reconstruction. Similar to standard bent-ray tomography[8], DD tomography algorithm iteratively solves the nonlinear inversion problem. At each iteration, the ray paths are updated using the newly modified sound speed model to incorporate ray bending effects. Details about our methods to solve forward and inverse problems are described as follows.

2.3 Forward modeling

The ultrasound wave from transmitter *i* arriving at receiver *k* at time *T* can be expressed using ray theory as a path integral

$$T_k^i = \int_i^k u ds \tag{1}$$

where *u* is slowness (inverse of sound speed) and *ds* is an element of ray path length. In forward modeling, we discretize the slowness (inverse of sound speed) field to equal sized rectangular grid cells[8]. We solve the 2-D eikonal equation using a grid travel-time tracing technique[9]

$$(\nabla E)^2 = (\partial T/\partial x)^2 + (\partial T/\partial y)^2 = (1/v)^2 = (s_x^2 + s_y^2)\,. \tag{2}$$

The (*x, y*) are discrete spatial grid coordinates, *T* is the travel-time, *v* is the sound-speed, and (s_x, s_y) is the slowness vector of the ultrasound wave that is defined as the inverse of sound speed. In eq. (2), $E = const.$ describes the 'wavefronts', and 'rays' are defined as the orthogonal trajectories of these wavefronts. The ray paths are traced using the slowness vector (s_x, s_y) that can be obtained by calculating the gradient of the travel-time field[8, 9].

2.4 Inverse problem

Let Δt_i be the difference between the *i*th picked ToF from the recorded ultrasound data and the *i*th calculated ToF for the sound speed model

$$\Delta t_i = t_i^{obs} - t_i^{cal}\,, \tag{3}$$

the traditional inverse problem can be described as follows

$$\sum_j^M l_{ij}\Delta s_j = \Delta t_i\,, \tag{4}$$

where Δs_j is the slowness perturbation for the *j*th grid cell, which needs to be inverted, and l_{ij} is the ray length of the *i*th ray within the *j*th cell. Equation (4) can be expressed as a matrix form

$$L\Delta S = \Delta T\,. \tag{5}$$

Subtracting a similar equation for a nearby ray k from equation (4), we have

$$\Delta t_i - \Delta t_k = \sum_j^M l_{ij}\Delta s_j - \sum_j^M l_{kj}\Delta s_j\,, \tag{6}$$

where $\Delta t_i - \Delta t_k$ is the so-called double difference[1-7]. This term describes the difference between observed and calculated differential ToFs for two nearby rays, and can also be written as

$$\Delta t_i - \Delta t_k = (t_i^{obs} - t_k^{obs}) - (t_i^{cal} - t_k^{cal}), \tag{7}$$

The observed differential ToFs $(t_i^{obs} - t_k^{obs})$ can be calculated from waveform cross correlation. Note that the waveforms of nearby rays for our toroidal array are similar, which results in more accurate cross correlation data for the reconstruction. Equation (6) can also be expressed in matrix form

$$DL\Delta S = D\Delta T, \tag{8}$$

where D, the differential operator matrix , has the following form

$$D = \begin{bmatrix} 1 & -1 & . & . & . & . \\ 1 & . & . & -1 & . & . \\ . & . & . & . & . & . \\ . & . & 1 & . & -1 & . \\ . & . & . & . & . & . \end{bmatrix}. \tag{9}$$

If we assume that $A=DL$ is the new kernel matrix and $\Delta TT = D\Delta T$ is the new data vector for the DD inversion problem, equation (9) becomes

$$A\Delta S = \Delta TT. \tag{10}$$

This is a nonlinear inverse problem due to ray bending and can be solved in a similar way as described in [8].

3. RESULTS

We apply DD tomography to data acquired from toroidal array scans of a breast phantom, a gelatin phantom and 6 excised mouse mammary glands. We compare the obtained sound speed images with those from standard tomography. The results are present as follows.

3.1 Breast phantom

An initial phantom study was conducted to evaluate the performance of the DD tomography method. The breast phantom was built by Dr. Ernest Madsen of the University of Wisconsin and provides tissue-equivalent scanning characteristics of highly scattering, predominantly parenchymal breast tissue. A X-ray CT scan was taken after the manufacture of the breast phantom (Fig. 2c) to benchmark its anatomical structure.

A comparison of the DD tomography result with standard tomography is shown in Fig. 2. The sound speed scale in Fig. 2a and 2b is from 1470 m/s to 1550 m/s. Structures in both the DD tomogram in Fig. 2a and the standard tomogram in Fig. 2b are generally consistent with the X-ray CT image in Fig. 2c. The ultrasound scanning position was not exactly matching the position in Fig. 2c, which partially explains the size mismatch of the inclusions between Figs. 2a, 2b and Fig. 2c.

Visual comparison of Fig. 2a to Fig. 2b shows that the DD tomogram demonstrates better resolution and sharper image as well as less random noise. We further assess the images in Figs. 2a and 2b quantitatively, and compare the calculated sound speeds with known sound speeds obtained during manufacture (Table I). The results show that the calculated sound speeds in the DD tomogram are more consistent with the known values, while sound speeds from standard tomography show larger discrepancies from known values. Accuracy of DD tomography mainly relies on relative time shift between waveforms which can be accurately estimated using cross correlation for waveforms with similar shape. Accuracy of standard tomography heavily depends on clear onset time of signal arrivals and precise estimation of system delays during data acquisition, both of which are more prone to errors than waveform cross-correlation.

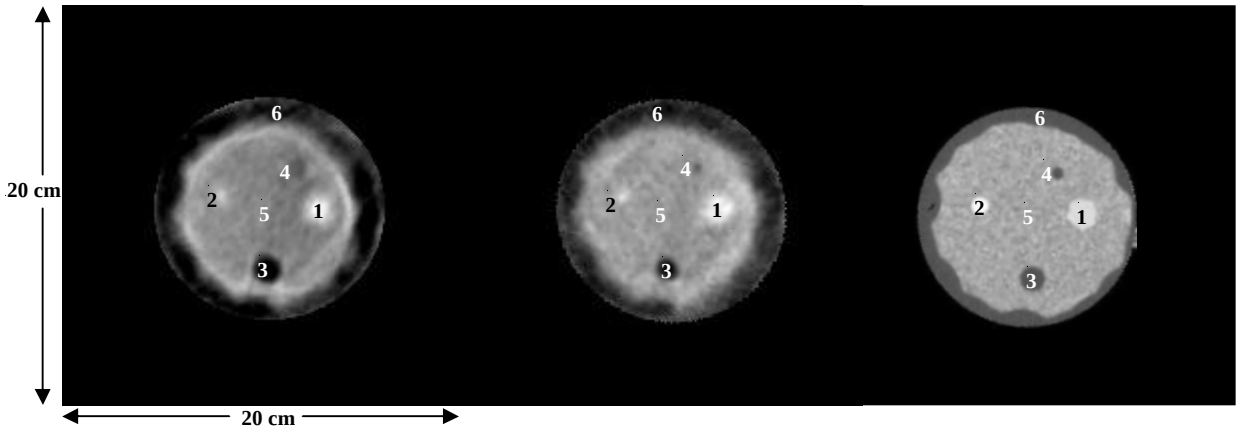

(a) Sound speed reconstruction with DD tomography

(b) Sound speed reconstruction with standard tomography

(c) X-ray CT scan

Figure 2. (a) Sound speed reconstruction with DD tomography for the breast phantom. (b) Sound speed reconstruction with standard tomography for the same cross section as in (a). (c) X-ray CT scan. 1 and 2: cancer; 3 and 4: fat; 5: granular tissue; 6: subcutaneous fat.

Table 1

Material number	Known sound speed (m/s)	DD tomography (m/s)	Standard tomography (m/s)
1	1549	1546	1534
2	1559	1535	1524
3	1470	1471	1464
4	1470	1500	1495
5	1515	1516	1507
6	1470	1475	1470

3.2 Gelatin phantom

A gelatin phantom (Fig. 3a) was prepared using plain gelatin powder with two embedded cherry tomatoes and one soft candy simulating rounded and irregular shaped inclusions. The phantom in Fig. 3a was scanned with our toroidal array from top to bottom for a total of 40 slices. We applied both DD tomography and standard tomography to the acquired data. Figures 3b and 3c present examples of sound speed images for selected slices. DD tomography generally gives sharper images when compared to standard tomography. In the resliced cross sections (images in lower part of Figs. 3b and 3c), DD tomography successfully reconstructs the irregular shaped soft candy (marked as 3) and the rounded tomato (marked as 2) that are indiscernible in the corresponding standard tomogram. The resliced tomograms show that, compared to standard tomography, DD tomography has higher out-of-plane resolution which is generally lower than in-plane resolution due to the nature of the toroidal array.

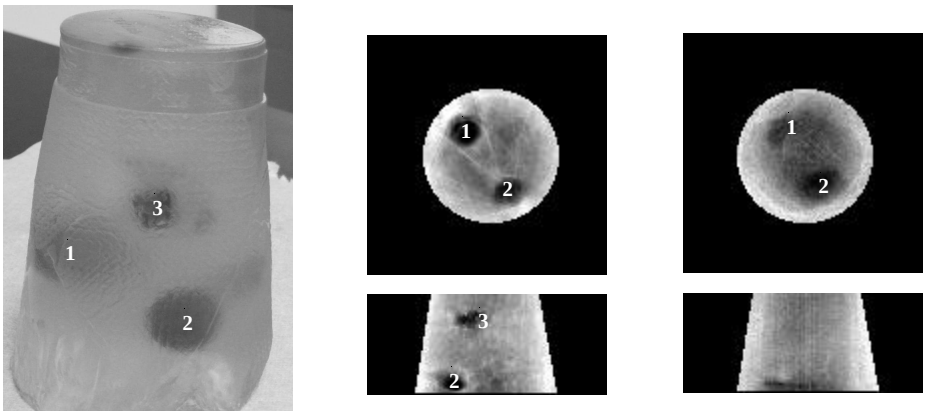

(a) Gelatin phantom (b) Sound speed reconstruction with DD tomography (c) Sound speed reconstruction standard tomography

Figure 3. (a) Gelatin phantom with one soft candy and two cherry tomatoes imbedded. (b) Sound speed reconstruction with DD tomography. (c) Sound speed reconstruction with standard tomography for the same cross section as in (b). In both (b) and (c), the upper images are cross sections in horizontal direction and the lower ones are resliced cross sections in vertical direction. 1: tomato 1; 2: tomato 2; 3: soft candy.

3.3 Excised mouse mammary glands data

We scanned 6 excised mouse mammary glands using our toroidal ring. In order to minimize the movements during the scan, the mammary glands were soaked in a mixture of alcohol and saline in a latex container. The density of the fluid mixture is similar to the mammary glands under interrogation so that the mammary glands can stay steadily in the middle of the container for a stable scan.

We applied DD tomography to the above 6 mouse mammary glands data. An example of a cross-sectional sound speed image for one mouse mammary gland is shown Fig. 4a (DD tomography), compared to sound speed image from standard tomography in Fig. 4b. The corresponding reflection image is presented in Fig. 4c for better comparison. The mammary gland in Fig. 4c (indicated by arrow) shows as low sound speed in the DD tomogram (Fig. 4a), while it is not detectable in the standard tomogram (Fig. 4b).

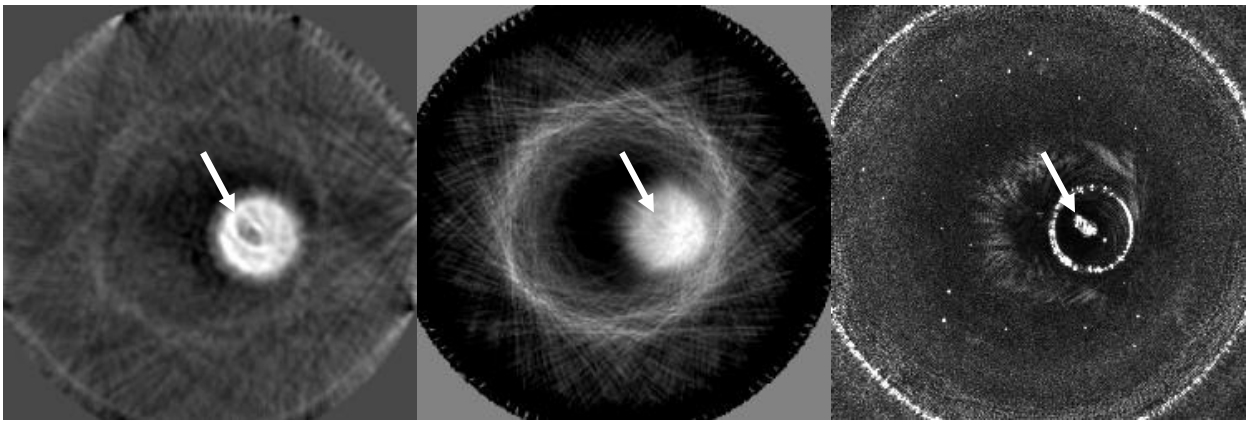

(a) Sound speed reconstruction with DD tomography

(b) Sound speed reconstruction with standard tomography

(c) Reflection image

Figure 4. (a) Sound speed reconstruction with DD tomography for an excised mouse mammary gland. (b) Sound speed reconstruction with standard tomography for the same cross section as in (a). (c) The corresponding reflection image. In (a) and (b) darker color stands for lower sound speed. The scale is the same as Fig. 1.

4. DISCUSSION AND CONCLUSIONS

We have developed a cross correlation based DD sound speed tomography algorithm for a toroidal ring. We have applied this algorithm to data for one breast phantom, one gelatin phantom and six excised mouse mammary glands, acquired using the toroidal ring. We compared sound speed images of DD tomography with those of standard tomography. Our results clearly demonstrate that DD reconstructions are superior to standard tomography reconstructions in terms of both resolution and accuracy. Standard tomography heavily depends on the quality of the ToF picks whose accuracies
rely on clear onset of the signal arrivals, while cross correlation used by DD tomography is more accurate to small time shifts between two waveforms without relying on the signal onset time. Two waveforms to be cross correlated must present similar shapes in order to get accurate relative time shift, which is by default satisfied by our toroidal acquisition geometry.

Another advantage of DD tomography, unlike standard tomography, is that the unknown systematic data acquisition delays are canceled out upon cross correlation and plays no effect on the final sound speed images. There have been many seismic applications using both DD location and DD tomography algorithms demonstrating that even using just the differences of ToF picks leads to significant improvement of event locations, as well as for the velocity structure. As discussed in [3] and [6], picking errors include two parts: random and systematic. Although random errors may increase through the differencing process, the systematic errors will be reduced or cancelled. This property of DD tomography ensures that the inversion problem is better conditioned and, consequently, more accurate sound speed values in the image can be obtained.

One technical difficulty for DD tomography is that we need to appropriately select a segment from each waveform for cross correlation in order to get accurate time difference. The segment selected needs to be short enough to avoid the effect of signals arriving later than the first signal pulse and long enough to avoid faulty cross correlation calculations. Strategies need to be developed to smartly select time windows for each waveform.

ACKNOWLEDGEMENTS

This work was supported in part by a research grant from the Michigan Economic Development Corporation (MEDC653) and Susan G. Komen Breast Cancer Foundation (KG100100).

REFERENCES

1. Waldhauser, F., Ellsworth, W. L., “A double difference earthquake location algorithm: Method and application to the Northern Hayward fault, California,” Bull. Seismol. Soc. Am., 90, 1353-1368 (2000).
2. Waldhauser, F., “hypoDD: A computer program to compute double-di erence hypocenter locations,” U.S. Geol. Surv. Open File Rep. 25, 01–113 (2001).
3. Zhang, H. and Thurber, C., “Double-Difference Tomography: The Method and Its Application to the Hayward Fault, California,” Bull. Seismol. Soc. Am., 93, 1875-1889 (2003).
4. Zhang, H., Ratchkovski, N., Thurber, C., and Hansen, R., “High-resolution seismic velocity structure of the Alaska subduction zone revealed by double-difference tomography,” EOS Trans. AGU (47), Fall Meet. Suppl., Abstract S51B–0168 (2004).
5. Zhang, H., and Thurber, C., “Adaptive-mesh seismic tomography based on tetrahedral and Voronoi diagrams: Application to Parkfield,” California, J. Geophys. Res. 110, B04303 (2005).
6. Zhang, H., Thurber, C., Shelly, D., Ide, S., Beroza, G. C., and Hasegawa, A., “Highresolution subducting-slab structure beneath northern Honshu, Japan, revealed by double-difference tomography,” Geology 32, 361–364 (2005).
7. Zhang, H. and Thurber, C., “Development and Application of Double-difference seismic Tomography,” Pure appl. Geophys., 163, 373-403 (2006).
8. Li, C., Duric, N., “In vivo breast sound-speed imaging with ultrasound tomography,” Ultrasound in Med. & Biol., 35, 1615-1628 (2009).
9. Klimes, L., “Grid Travel-time Tracing: Second-order Method for the first Arrivals in Smooth Media,” Pageoph, 148, 539-563 (1996).